ChemComm

ROYAL SOCIETY OF CHEMISTRY

COMMUNICATION

View Article Online
View Journal | View Issue

Cite this: *Chem. Commun.*, 2024, **60**, 11128

Received 11th July 2024,
Accepted 5th September 2024

DOI: 10.1039/d4cc03461a

rsc.li/chemcomm

Zinc triazolate oxalate CALF-20 with platelet morphology and its PEBAX-based mixed matrix membranes for CO_2/N_2 separation†

Qian Jia, ‡[a] Elsa Lasseuguette, ‡[b] Harpreet Kaur,[a] Aaron B. Naden,[a] Maria-Chiara Ferrari*[b] and Paul A. Wright *[a]

CALF-20, [Zn_2(1,2,4-triazolate)$_2$(oxalate)] shows remarkable performance in post-combustion carbon capture, even under humid conditions[1] but its reported crystal morphology hinders its applicability in mixed matrix membranes (MMMs). Here, a route to its preparation as platelets a few tens of nm thick is reported. These were incorporated into a PEBAX MH1567 polymer matrix and the resultant MMMs display improvement in CO_2 permeability and CO_2/N_2 selectivity.

The removal and concentration of CO_2 from mixed gas streams is important for current and future carbon capture applications. The use of solid adsorbents rather than amine solutions for this offers many potential advantages, particularly if CO_2 can be adsorbed selectively over N_2 in the presence of moisture and at low CO_2 partial pressure.[1] Among those materials being investigated for carbon capture, metal organic frameworks (MOFs), a large and expanding family of porous crystalline solids comprising metal cations and organic linkers, are of particular importance due to their large surface areas and tuneable surfaces.[2] Some MOFs not only show structural stability to moisture but also retain capacity for CO_2 in moist gas streams[3] where zeolites are rapidly deactivated. Among those receiving most attention for carbon capture are the amine-appended large pore Mg carboxylate Mg-MOF-74R,[4] the pillared niobium oxyfluoride NbOFFive[5] and the zinc triazolate oxalate CALF-20 (Calgary Framework 20, Zn_2(1,2,4-triazole)$_2$(oxalate)).[1] CALF-20 consists of zinc triazolate layers pillared by oxalate linkers (Fig. 1), and has recently been shown to adopt one of two closely related structures, α or β, depending on the partial pressure of water.[6] At relative humidity below 23% the widely described α-form is observed, whereas at higher relative humidity the β-form is stable. Upon the reversible phase transformation from α to β, the oxalate groups tilt relative to the zinc triazolate layers and their binding changes from bis-bidentate to bis-monodentate-dominant; there is also a distortion of the $Zn_2(trz)_2$ pore opening.

CALF-20 has excellent CO_2 uptake at room temperature at a few percent of CO_2 and exhibits high CO_2/N_2 selectivity and long term stability in the presence of moisture, notwithstanding the α to β transition.[6] In addition, its small pores function as CO_2 adsorbents at relative humidities at which the pores of zeolites would fill with water.[6] While carbon capture using packed beds of CALF-20 in pressure and temperature swing processes has been proposed, membrane technology could also make use of this MOF. Polymeric membranes have been widely investigated for gas separation, but suffer from ageing effects as well as the trade-off between gas permeability and selectivity described by the Robeson upper bound.[7] To surpass this limit, a mixed matrix strategy of incorporating nanoporous solid

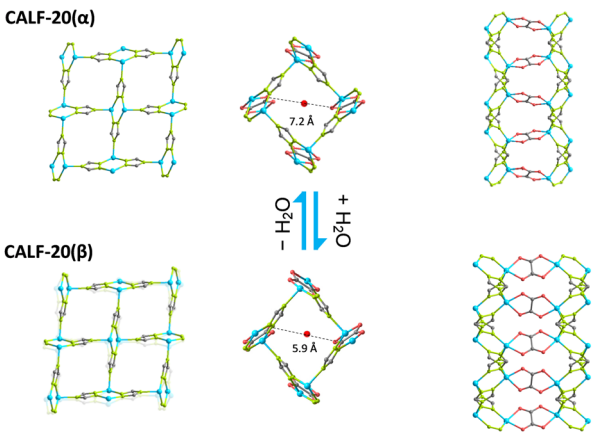

Fig. 1 The α and β forms of CALF-20, showing for each (left to right) the $Zn_2(trz)_2$ layer; intralayer aperture and pillared structure (Zn blue; N green; C, grey; O, red).

[a] *EaStCHEM School of Chemistry, University of St Andrews, Purdie Building, North Haugh, St Andrews KY16, 9ST, UK. E-mail: paw2@st-andrews.ac.uk*
[b] *School of Engineering, University of Edinburgh, Robert Stevenson Rd, Edinburgh EH9 3FB, UK. E-mail: M.Ferrari@ed.ac.uk*

† Electronic supplementary information (ESI) available. See DOI: https://doi.org/10.1039/d4cc03461a

‡ These authors contributed equally to this work.

fillers into a polymer matrix has been shown to enhance performance.[8–10] Some of the best studied examples involve the use of zeolitic imidazolate frameworks (ZIFs) as fillers, due to their chemical and structural variety and their ease of preparation as nanocrystals.[10]

CALF-20 has previously been incorporated within Nafion for CO_2/N_2 separation, but its particle size (*ca.* 1 μm) and blocky morphology results in a low volume occupation and poor filler distribution, and consequently low CO_2/N_2 selectivity (α_{CO_2/N_2} = 2.1 for a mixed gas stream with 10% CO_2 and 90% N_2).[11] Modifying its crystal morphology could improve its performance in MMMs. One possibility would be to prepare it in nanoplatelet form, as a '2D MOF'. There has been much recent attention paid to the applications of 2D MOFs in MMMs, because their high aspect ratio enables fast transport for favoured gas species while increasing greatly the tortuosity for non-favoured molecules, even at low filler loadings (below 10 wt%).[12] The crystal structure of CALF-20 is strongly anisotropic, so that it was expected that it would be amenable to preparation as platelets under suitable conditions of crystal growth. Other studies have shown that ZIF-8 platelets can be prepared by careful use of a lamellar zinc-bearing precursor $Zn_5(OH)_8(NO_3)_2{\cdot}2H_2O$[13] (Fig. S1, ESI†) and these show attractive properties as MMM fillers.[14] Here, we report a synthesis route to CALF-20 which uses that lamellar zinc-containing precursor and gives platelets a few tens of nm thick, and we incorporate these within PEBAX-MH1657 to obtain MMMs that show enhancement in CO_2 permeability and CO_2/N_2 selectivity, even at low filler content.

CALF-20 crystallised at room temperature from a mixture of oxalic acid, triazolate and basic zinc carbonate in a water/ethanol solution,[1] gives micron-sized crystals that are not suitable for MMM fillers (Fig. S2a, ESI†). This CALF-20(lit), dried at 60 °C overnight, and run in a capillary in Debye–Scherrer geometry gave the PXRD pattern reported for CALF-20(α) and predicted from the crystal structure[1] (Fig. 2a).

We investigated the use of $Zn_5(OH)_8(NO_3)_2{\cdot}2H_2O$ as a zinc precursor with a layered structure in the synthesis, with the aim that this would promote crystallisation of CALF-20 with platelet morphology. $Zn_5(OH)_8(NO_3)_2{\cdot}2H_2O$, which has a layered crystal structure with a positively charged zinc hydroxide layer and intercalated nitrate anions (Fig. S1, ESI†), was prepared by reacting $Zn(NO_3)_2$ and Li(OH) solutions according to the published procedure (ESI†).[13] This zinc hydroxide nitrate was used in subsequent reaction with 1,2,4-triazole and oxalic acid in methanolic solution *via* microwave heating at 90 °C for 1.5 h and the product washed and dried. SEM indicated the product CALF-20 has platelet morphology with a crystallite dimension across the thin plates of around one micron (Fig. 3a and b). The platelets were examined by AFM, giving an estimated thickness of around 30 nm (Fig. 3c and d) and an aspect ratio of 22. It should be noted that the use of the layered zinc hydroxide nitrate precursor, rather than elevated temperature, is critical for the synthesis of platelets: microwave heating of the gel prepared using basic zinc carbonate as the zinc source gave bulky crystals of CALF-20 (Fig. S2b, ESI†) that were in the α-form (Fig. S3, ESI†).

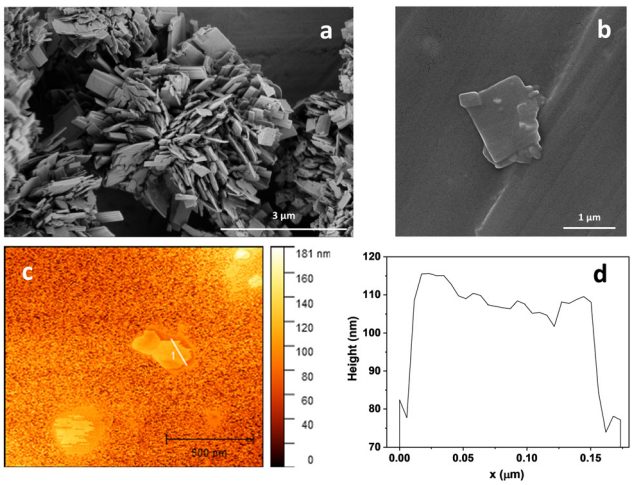

Fig. 3 SEM images of (a) platy CALF-20, and (b) exfoliated CALF-20 plates, (c) AFM image of single CALF-20 plate and (d) the height profile of CALF-20 plate along the line in (c).

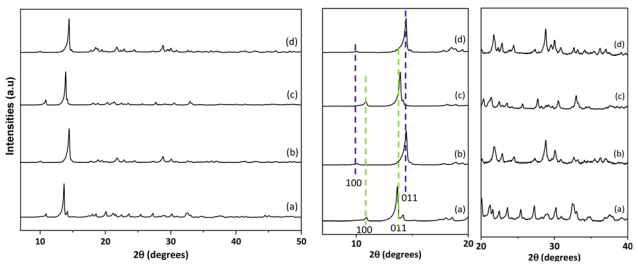

Fig. 2 PXRD (measured with Mo $K_{\alpha 1}$ and represented as if from Cu $K_{\alpha 1}$) of (a) CALF-20(lit), (b) CALF-20(P), (c) CALF-20(P) under vacuum and (d) rehydrated (indexed peaks in green for CALF-20(α) and purple for CALF-20(β), respectively).

PXRD of the platelets showed differences from that of the CALF-20(α) prepared *via* the literature method (Fig. 2). Indexing gave a unit cell of 9.33 Å × 8.00 Å × 10.00 Å, close to that reported for CALF-20(β)[6] and comparison of the PXRD against that calculated for CALF-20(β) indicated it was CALF-20(β) (Fig. S4, ESI†). As CALF-20(β) is reported to transform reversibly to the α-form upon drying, a sample was loaded in a capillary, evacuated (10^{-4} mbar) at room temperature and sealed. PXRD showed the structure had transformed to the α-form. The capillary was then broken and overnight exposure of the powder to moist lab air resulted in transformation back to CALF-20(β). That the β-form is observed during initial characterisation of the platelets but not the bulky crystals prepared *via* the literature method is remarkable. It is likely that the α-form results from drying both morphologies, but the CALF-20 platelets transform to the β-form more rapidly upon exposure to moisture when loading capillaries due to faster H_2O uptake *via* shorter diffusional paths.

The CO_2 adsorption isotherm at 298 K of the platy CALF-20 (referred to here as CALF-20(P)) up to 1 bar is very close to that measured for the bulky crystals prepared *via* the literature

method (Fig. S5a, ESI†). Further, CO_2 and N_2 adsorption isotherms up to 10 bar at 298 K (Fig. S5b, ESI†) are very similar to those reported for CALF-20.[1] At 1.2 bar the corresponding CO_2 uptake and CO_2/N_2 selectivity are 4.22 mmol g^{-1} and 8.6, respectively. The thermal behaviour of CALF-20(P) and the CALF-20 prepared *via* the literature method were examined under air (Fig. S6a, ESI†). Both start decomposing at 600 K, leaving a residue that accounts for 42 wt% of total mass, consistent with reported data. FTIR spectra (Fig. S6b, ESI†) confirm the materials' similarity.

To prepare MMMs using CALF-20(P) as filler, a suspension of the platelets in methanol was ultrasonicated to produce more single platelets, as observed by SEM and AFM (Fig. 3 and Fig. S7, ESI†) and TEM (Fig. S8, ESI†). MMMs were prepared by incorporating 3 to 10 wt% CALF-20 platelets into PEBAX MH1657 *via* a solution/slow evaporation method described in the ESI.† Membranes based on the neat polymer were prepared similarly. The thickness of all membranes was *ca.* 50 μm. PXRD of MMMs (Fig. S9, ESI†) confirms that the CALF-20 filler retains structure and crystallinity after combining with PEBAX. By comparison with conventional MOF particle fillers, the loading for 2D MOF-containing MMMs is typically from 2 to 10 wt%.[15] The high loading limitation originates from the tendency of 2D materials to agglomerate at higher content due to their high surface energy.[16] Despite the low content, their high aspect ratio allows more efficient dispersion within the membrane compared to 3D materials. Fig. S10 (ESI†) displays the microstructure of the MMMs. Pure PEBAX is smooth, while the incorporation of filler increases the MMMs' roughness without introducing defects over the loading range 3–10 wt%. Up to 7 wt%, the CALF-20 fillers are homogeneously distributed. At 10 wt%, a high loading of CALF-20 filler induces severe settling (Fig. S10j, ESI†) at the bottom of the membrane due to the greater density of CALF-20 fillers (1.8 g cm^{-3}) compared to that of the polymeric solution (1.1 g cm^{-3}). The distribution of CALF-20 fillers was also examined by focused ion beam scanning electron microscopy (FIB-SEM), and a representative cross-section of MMMs at 7 wt% loading is shown in Fig. 4a, indicating the morphology of the filler is unchanged by incorporation in the membrane. The incorporation of platy CALF-20 within MMMs was shown to be homogeneous by elemental mapping of Zn (Fig. S11, ESI†)

TGA (Fig. S12, ESI†) indicates that MOF fillers have a small impact on membrane thermal stability in general, but increasing the filler loading can accelerate membrane decomposition at lower temperature.

The permeation of pure N_2 and CO_2 gases through neat polymer membrane and the MMMs was assessed at 1.2 bar absolute and 293 K. Fig. 4b indicates that up to 7 wt% the incorporation of CALF-20 fillers significantly enhances both CO_2 permeability and CO_2/N_2 selectivity, by about 37% and 67%, respectively, approaching the Robeson 2008 upper bound (Fig. S13, ESI†).[12] The MMMs with 3 and 5 wt% CALF-20 demonstrate good performance compared to MMMs with other loadings, but also in comparison with PEBAX mixed with other fillers.[17] At 10 wt%, a dramatic drop is observed in both CO_2

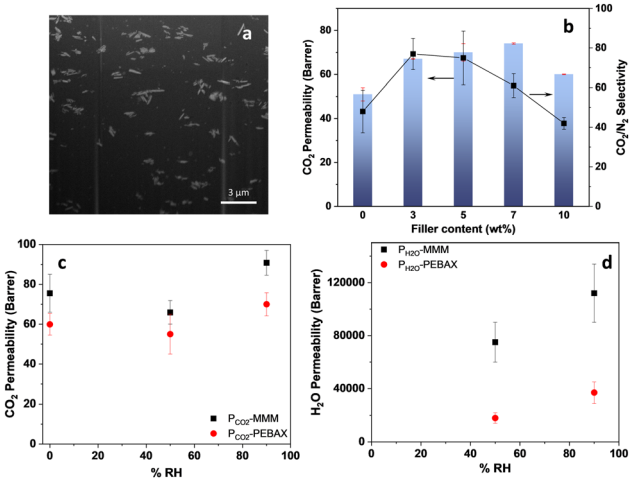

Fig. 4 (a) FIB-SEM cross-section of MMM with 7 wt% CALF-20(P), (b) CO_2 permeability (blue bars) and CO_2/N_2 selectivity (black squares) for MMMs with CALF-20 at different loadings, (c) CO_2 permeability and (d) H_2O permeability *vs.* feed humidity (%RH) for PEBAX (red circle) and PEBAX_-CALF-20_5 wt% (black rectangle).

permeability and selectivity, which we attribute to the reduced effect of CALF-20(P) that results from the high degree of agglomeration and settling.

Membrane diffusivity and solubility were determined, to investigate the filler effects on membrane performance, as described in the ESI† and depicted in Fig. S14. Diffusivity coefficients decrease gradually with increasing filler, attributed to the MOF's impact on polymer chain packing and rotational mobility. Additionally, the predicted CO_2 diffusivity coefficient in pure CALF-20 is 1×10^{-7} cm^2 s^{-1},[18] lower than the diffusivity in PEBAX (2.6×10^{-7} cm^2 s^{-1}).[19] Therefore, the overall diffusivity in MMMs decreases due to the increased hindrance from fillers. However, incorporating CALF-20 fillers leads to a marked improvement in CO_2 solubility. For example, a five-fold enhancement is realised at 5 wt%, ascribed to the strong affinity of CALF-20 to CO_2, resulting in an overall increase of CO_2 permeability. The CO_2 solubility derived from the permeation measurement with the MMMs at 7 wt% is consistent with the membrane sorption isotherm (Fig. S15 and Table S2, ESI†). Further, to validate the impact of CALF-20 morphology on membrane performance, a modified Maxwell model was applied to predict gas permeation of 2D-filler-incorporated MMMs.[20,21] Using eqn (S7) (ESI†) for this model, where the shape factor is expressed as G (for spherical fillers, G is equal to 2, while for lamellae, G tends to infinity as an indication of low hindrance). CALF-20(P) MMMs give a G of 50 for predicting CO_2 transport (Fig. S16, ESI†).

In addition to dry gas permeation measurements, CO_2 permeation data under wet conditions (pure CO_2 with 50% and 90%RH, see Scheme S2, ESI†) for PEBAX and PEBAX-CALF-20-5 wt% have been carried out (Fig. 4c and d). The CO_2 permeability of the PEBAX (60 Barrer at 0% RH) decreases (50%RH, 55 Barrer) then increases (90% RH, 70 Barrer). A similar trend is observed for PEBAX_CALF-20_5%. This might

be explained by competitive sorption effects at low humidity content, inhibiting the CO_2 permeation. However, at higher humidity content, the water molecules induce the swelling of the PEBAX, resulting in a higher gas flux. Even in the presence of water, PEBAX_CALF-20_5% exhibits a larger CO_2 permeation than PEBAX. H_2O permeability follows the same trend for PEBAX and MMMs, with an increase of the water permeability with feed humidity content (Fig. 4d) due to an increase of water sorption at higher activities.[22]

CALF-20 holds great promise for selective MMMs due to its high CO_2 uptake and stability in the presence of moisture. However, the bulky morphology of CALF-20 is not suitable for incorporation into polymer membranes. Here, we present a route to platelet CALF-20 (aspect ratio 22) by using layered zinc hydroxide nitrate as a precursor and with microwave heating. This CALF-20 exhibits comparable CO_2 and N_2 uptake with that synthesised *via* literature methods but its morphology enables homogeneous incorporation within PEBAX polymer matrix at 3–7 wt%, giving enhancement in CO_2 permeability and CO_2/N_2 selectivity and an overall performance that approaches the 2008 Robeson upper bound. In the presence of water, CO_2 permeability of the MMM was also enhanced compared to pure PEBAX membrane.

QJ acknowledges funding from the CSC scheme from the Chinese Government (201908140117); EL and M-CF thank EPSRC (SynHiSel, EP/V047078/1); HK and PAW acknowledge funding from the UKRI (UKRI, Soldac, ISF no. 10038044). The authors also acknowledge the EPSRC for grants EP/L017008/1 (TEM), EP/V034138/1 (PXRD, Core Equipment Grant) and EP/R023751/1 (Strategic Equipment Grant) to the University of St Andrews.

Data availability

Additional information and data is given in the ESI† and the raw data supporting this publication can be accessed at **https://doi.org/10.17630/d3691837-273f-48ea-8356-96552e8019fd**.

Conflicts of interest

There are no conflicts to declare.

Notes and references

1 J.-B. Lin, T. T. T. Nguyen, R. Vaidhyanathan, J. Burner, J. M. Taylor, H. Durekova, F. Akhtar, R. K. Mah, O. G. Nik, S. Marx, N. Fylstra, S. S. Iremonger, K. W. Dawson, P. Sarkar, P. Hovington, A. Rajendran, T. K. Woo and G. K. H. Shimizu, *Science*, 2021, **374**, 1464–1469.
2 C. A. Trickett, A. Helal, B. A. A. Maythalony, Z. H. Yamani, K. E. Cordova and O. M. Yaghi, *Nat. Rev. Mater.*, 2017, **2**, 17045.
3 C. Wang, X. Liu, N. Keser Demir, J. P. Chen and K. Li, *Chem. Soc. Rev.*, 2016, **45**, 5107–5134.
4 R. Hughes, G. Kotamreddy, A. Ostace, D. Bhattacharya, R. L. Siegelman, S. T. Parker, S. A. Didas, J. R. Long, B. Omell and M. Matuszewski, *Energy Fuels*, 2021, **35**, 6040–6055.
5 S. Ullah, K. Tan, D. Sensharma, N. Kumar, S. Mukherjee, A. A. Bezrukov, J. Li, M. J. Zaworotko and T. Thonhauser, *Angew. Chem. Int. Ed.*, 2022, **61**, e202206613.
6 Z. Chen, C.-H. Ho, X. Wang, S. M. Vornholt, T. M. Rayder, T. Islamoglu, O. K. Farha, F. Paesani and K. W. Chapman, *ACS Mater. Lett.*, 2023, 2942–2947.
7 H. B. Park, J. Kamcey, L. M. Robeson, M. Elimelech and B. D. Freeman, *Science*, 2017, **356**, 6343; L. M. Robeson, *J. Membr. Sci.*, 2008, **320**, 390–400.
8 B. Seoane, J. Coronas, I. Gascon, M. E. Benavides, O. Karvan, J. Caro, F. Kapteijn and J. Gascon, *Chem. Soc. Rev.*, 2015, **44**, 2421–2454.
9 Z. Wang, D. Wang, S. Zhang, L. Hu and J. Jin, *Adv. Mater.*, 2016, **28**, 3399–3405.
10 M. E. Benavides, O. David, T. Johnson, M. M. Lozinska, A. Orsi, P. A. Wright, S. Mastel, R. Hillenbrand, F. Kapteijn and J. Gascon, *J. Membr. Sci.*, 2018, **550**, 198–207.
11 T. A. Attas, S. K. Nabil, A. S. Zeraati, H. S. Shiran, T. Alkayyali, M. Zargartalebi, T. Tran, N. N. Marei, M. A. A. Bari, H. Lin, S. Roy, P. M. Ajayan, D. Sinton, G. Shimizu and M. G. Kibria, *ACS Energy Lett.*, 2023, **8**, 107–115.
12 Y. Pu, Z. Yang, V. Wee, Z. Wu, Z. Jiang and D. Zhao, *J. Membr. Sci.*, 2022, **641**, 119912; T. Rodenas, I. Luz, G. Prieto, B. Seoane, H. Miro, A. Corma, F. Kapteijn, F. X. L. Xamena and J. Gascon, *Nat. Mater.*, 2015, **14**, 48–55; X. Feng, Z. Qin, Z. Zhang, Z.-W. Shao, W. Tang, W. Wu, Z. Dai and C. Liu, *Sep. Purif. Technol.*, 2023, **305**, 122476.
13 P. Li, Z. P. Xu, M. A. Hampton, D. T. Vu, L. Huang, V. Rudolph and A. V. Nguyen, *J. Phys. Chem. C*, 2012, **116**, 10325–10332.
14 O. Kwon, M. Kim, E. Choi, J. H. Bae, S. Yoo, J. C. Won, Y. H. Kim, J. H. Shin, J. S. Lee and D. W. Kim, *Sci. Adv.*, 2022, **8**, eabl6841.
15 J. Winarta, A. Meshram, F. Zhu, R. Li, H. Jafar, K. Parmar, J. Liu and B. Mu, *J. Polym. Sci.*, 2020, **58**, 2518–2546.
16 Z. Hu, E. M. Mahdi, Y. Peng, Y. Qian, B. Zhang, N. Yan, D. Yuan, J.-C. Tan and D. Zhao, *J. Mater. Chem. A*, 2017, **5**, 8954–8963.
17 W. Zheng, R. Ding, K. Yang, Y. Dai, X. Yan and G. He, *Sep. Purif. Technol.*, 2019, **214**, 111–119; Q. Zhang, M. Zhou, X. Liu and B. Zhang, *J. Membr. Sci.*, 2021, **636**, 119612; P.-H. Tang, P. B. So, W.-H. Li, Z.-Y. Hui, C.-C. Hu and C.-H. Lin, *Membranes*, 2021, **11**, 404.
18 Y. Magnin, E. Dirand, G. Maurin and P. L. Llewellyn, *ACS Appl. Nano Mater.*, 2023, **6**, 19963–19971.
19 Q. Jia, E. Lasseuguette, M. M. Lozinska, M.-C. Ferrari and P. A. Wright, *ACS Appl. Mater. Interfaces*, 2022, **14**, 46615–46626.
20 L. G. Toy, B. D. Freeman, R. J. Spontak, A. Morisato and I. Pinnau, *Macromolecules*, 1997, **30**, 4766–4769.
21 Y. Eremin, A. Grekhov and A. Belogorlov, *Membranes*, 2022, **12**, 1100.
22 H. Sijbesma, K. Nymeijer, R. van Marwijk, R. Heijboer, J. Potreck and M. Wessling, *J. Membr. Sci.*, 2008, **313**, 263–276.